


Proton pencil beam scanning for mediastinal lymphoma: treatment planning and robustness assessment

Chuan Zeng, John P. Plastaras, Paul James, Zelig A. Tochner, Christine E. Hill-Kayser, Stephen M. Hahn & Stefan Both


To cite this article: Chuan Zeng, John P. Plastaras, Paul James, Zelig A. Tochner, Christine E. Hill-Kayser, Stephen M. Hahn & Stefan Both (2016) Proton pencil beam scanning for mediastinal lymphoma: treatment planning and robustness assessment, Acta Oncologica, 55:9-10, 1132-1138, DOI: [10.1080/0284186X.2016.1191665](https://doi.org/10.1080/0284186X.2016.1191665)


To link to this article: <https://doi.org/10.1080/0284186X.2016.1191665>

 View supplementary material [↗](#)


 Published online: 22 Jun 2016.

 Submit your article to this journal [↗](#)

 Article views: 1441

 View related articles [↗](#)

 View Crossmark data [↗](#)

 Citing articles: 9 View citing articles [↗](#)

ORIGINAL ARTICLE

Proton pencil beam scanning for mediastinal lymphoma: treatment planning and robustness assessment

Chuan Zeng^a, John P. Plastaras^a, Paul James^a, Zelig A. Tochner^a, Christine E. Hill-Kayser^a, Stephen M. Hahn^{a,b} and Stefan Both^a

^aDepartment of Radiation Oncology, University of Pennsylvania Perelman School of Medicine, Philadelphia, PA, USA; ^bDivision of Radiation Oncology, University of Texas MD Anderson Cancer Center, Houston, TX, USA

ABSTRACT

Background: Modern radiotherapy (RT) for lymphoma is highly personalized. While advanced imaging is largely employed to define limited treatment volumes, the use of proton pencil beam scanning (PBS) for highly conformal lymphoma RT is still in its infancy. Here, we assess the dosimetric benefits and feasibility of PBS for mediastinal lymphoma (ML).

Materials and methods: Ten patients were planned using PBS for involved-site RT. The initial plans were calculated on the average four-dimensional computed tomography (4D-CT). PBS plans were compared with 3D conformal radiotherapy (3D-CRT), intensity-modulated radiotherapy (IMRT), and proton double scattering (DS). In order to evaluate the feasibility of PBS and the plan robustness against inter- and intra-fractional uncertainties, the 4D dose was calculated on initial and verification CTs. The deviation of planned dose from delivered dose was measured. The same proton beamline was used for all patients, while another beamline with larger spots was employed for patients with large motion perpendicular to the beam.

Results: PBS provided the lowest mean lung dose (MLD) and mean heart dose (MHD) for all patients in comparison with 3D-CRT, IMRT, and DS. For eight patients, internal target volume (ITV) $D_{98\%}$ was degraded by <3%; and the MLD and MHD deviated by <10% of prescription over the course of treatment when the PBS field was painted twice in each session. For one patient with target motion perpendicular to the beam (>5 mm), the degradation of ITV $D_{98\%}$ was 9%, which was effectively mitigated by employing large spots. One patient exhibited large dose degradation due to pericardial effusion, which required replanning across all modalities.

Conclusions: This study demonstrates that PBS plans significantly reduce MLD and MHD relative to 3D-CRT, IMRT, and DS and identifies requirements for robust free-breathing ML PBS treatments, showing that PBS plan robustness can be maintained with repainting and/or large spots.

ARTICLE HISTORY

Received 11 November 2015
Revised 12 May 2016
Accepted 14 May 2016
Published online 21 June 2016

Introduction

Modern radiotherapy (RT) for lymphoma is highly personalized. Proton therapy enhances the ability to deliver conformal radiation treatments while sparing surrounding normal tissues. For mediastinal lymphoma (ML), passive scattering proton therapy has been shown to deliver a conformal dose to the tumor while decreasing dose to normal tissues like lung, esophagus, heart, and coronary arteries [1–3].

While advanced imaging is largely employed to define limited treatment volumes, the use of proton pencil beam scanning (PBS) for highly conformal lymphoma RT is still in its infancy. Although PBS has been the most advanced delivery method of proton therapy for two decades, previous reports of proton therapy on lymphoma have been limited to passive scattering, with the exception of several dosimetric study on PBS (e.g. [3,4]) which did not actually treat patients with PBS. Due to its time structure, beam scanning is more susceptible to intra-fractional motion when compared with passive scattering [5]. However, PBS has the ability to conform to the

target three-dimensionally. Therefore, PBS has potential to further limit the amount of irradiated normal tissue compared to passively scattered protons, and thus further reduce the risk of long-term complications. PBS also reduces the amount of potential neutrons in the field as no beam-shaping device is needed [6]. Deployment of PBS for ML treatment has been limited due to the lack of comprehensive assessment of PBS parameters in conjunction with patient-specific four-dimensional (4D) data. The simultaneous motion of organs and proton beams, referred to as the interplay effect [7], results in degradation of the dose distribution on target and/or organs at risk (OAR). One commonly considered strategy to mitigate the interplay effect is repainting, i.e. scanning repetitively within one fraction [8]. A number of repainting schemes have been investigated previously [9–11].

In previous studies, the breathing pattern has been simulated with mathematical functions; and the breathing period was assumed to be constant. Very recently, we reported on the impact of interplay that incorporated each patient's

respiratory trace instead of a simulated motion [12]. Moreover, the real-world problem of inter-fractional variation has not addressed in previous studies on interplay effect. In this study, we evaluate (1) the potential of proton PBS to increase OAR sparing in ML radiation relative to 3D conformal radiotherapy (3D-CRT), intensity-modulated radiotherapy (IMRT), and proton double scattering (DS); and (2) the interplay effect on both the planning 4D computed tomography (4D-CT) scans and verification 4D-CT scans, thus quantifying the impact of both intra- and inter-fractional motion, including setup, anatomical, and physiological changes, on proton PBS plan robustness for ML. The energy switching time τ_{switch} —the time required to vary the beam energy to conform the dose in depth—was varied across a range of relevant values in order to assess its potential impact on the dose distribution.

Materials and methods

Patient selection and 4D-CT simulation

Ten consecutive patients treated for ML at the Hospital of the University of Pennsylvania with DS proton therapy, who had at least two 4D verification CT scans, were included in this IRB-approved registry study.

All patients underwent 4D-CT simulation in the supine position. In addition, each patient underwent two to three verification 4D-CT scans over the course of treatment, typically every other week. The average interval between consecutive 4D-CTs was 15 days for the cohort. The respiratory phase was monitored during 4D-CT with the Varian Real-time Position Management (RPM) system (Varian Medical Systems, Palo Alto, CA). The target size, breathing characteristics, and target motion amplitudes of each patient were summarized in Supplementary Table S.I (available online at <http://www.informahealthcare.com>).

Treatment planning

The averages of the simulation 4D-CT scans were used for treatment planning in this study; we referred to this planning CT as the ‘initial average CT (IACT)’. The clinical target volumes (CTVs) were delineated according to the International Lymphoma Radiation Oncology Group guidelines [13,14] by the same attending physician, and were expanded based on their interphase displacements to generate the internal target volumes (ITVs). Explicitly, the ITVs were constructed from the union of CTVs from all motion phases of 4D-CTs. A volume for optimization purposes was defined as an anisotropic expansion of ITV with 0.5 cm in all directions, except the margins along the beam direction employed to correct upfront for the range uncertainty which can be a concern in proton therapy [15]. At our institution we applied a margin in the beam direction that was 3.5% of beam range (from skin) to correct for the uncertainties associated with CT imaging and conversion from CT numbers to water-equivalent depth, and an additional 1 mm to correct for the uncertainties in patient setup and detection of the skin surface [6,16]. The minimum range margin applied in this study was 0.5 cm regardless of range.

We investigated 17 fractions that deliver 30.6 Gy(RBE) to a corresponding target, i.e. 1.8 Gy(RBE)/fx. The PBS plan employed a single anterior field for each patient, which was in contrast to opposed PBS fields modeled in other studies [4,17]. The treatment planning system (TPS) Eclipse 11.0 (Varian Medical System) was used. As lymphoma targets tended to be shallow, a range shifter was applied in the beam path in order to further reduce the minimum beam energy of 100 MeV available at our institution.

We considered volumetric repainting so that, as applied in our clinic, at each treatment session the same field would be delivered twice. Thus, half of the prescription was applied to our treatment plans as $0.9\text{Gy (RBE)}/\text{fx} \times 17\text{fx} = 15.3\text{Gy(RBE)}$. The planning objective for the ITV was at least 98% of its volume received 97% of the prescription dose. The dose calculation within the TPS did not account for motion. We thus, for clarity, referred to the dose calculated in the original plan as the nominal dose distribution.

To assess dosimetric differences, each nominal PBS plan was compared with 3D-CRT, IMRT, and DS, generated by an experienced dosimetrist on the IACT. The objectives for OARs were: lung $V_{\text{mean}} \leq 15\text{Gy (RBE)}$, $V_{20\text{Gy(RBE)}} \leq 30\%$; heart $D_{\text{max}} \leq 30\text{Gy(RBE)}$, $D_{\text{mean}} \leq 5\text{Gy(RBE)}$. The 3D-CRT plan employed opposed fields (anterior-posterior). The IMRT plan employed 4–5 fields; oblique fields as well as non-coplanar fields were used when deemed necessary. Five millimeter planning target volume (PTV) expansion was used for the photon plans. This choice of PTV expansion was established from our practice of daily kV/kV imaging. It reflected our setup error and anatomy differences as documented by the verification CTs. DS plan typically employed a single anterior field, while another superior-anterior field may be chosen based on each patient’s anatomy. Similar to the PBS plan, the margins along the beam direction were based on calculated range uncertainty, which in turn depended on the proton beam range and modulation. The smearing was calculated based on motion magnitude and setup uncertainty. The PBS dose distribution depended on the range margin used as well. However, no correction for mechanical devices such as apertures and compensators would be needed for PBS. The lateral margin was determined by beam lateral penumbra width and setup and motion uncertainties. All proton doses included a mean relative biological effectiveness of 1.1 [6].

4D-evaluation

Respiratory traces and irradiation time

The respiratory traces recorded at each 4D-CT scan were used to establish the relation between breathing phases and time. Specifically, we used the phase-time relation generated by the RPM system.

Besides respiratory traces, the proton irradiation timing of beam spots within each iso-energy layer and across different layers needed to be determined, in order to simulate the interplay effect. This was calculated from the beam delivery sequence simulated by the vendor, in which the treatment plans were translated into equipment settings [12].

Simulation of the interplay effect

For each beam delivery sequence and initial breathing phase at which scanning commenced, the beam spots delivered in each phase were identified. In our clinic, 4D-CT data were binned into eight phases, denoted as 0% [end of inhalation (EI)], 12.5%, 25% [middle of exhalation (ME)], 37.5%, 50% [end of exhalation (EE)], 62.5%, 75% [middle of inhalation (MI)], and 87.5%. With the beam spots from one plan partitioned onto different phases of the 4D-CT, the dose was calculated on each phase. This was implemented by binning the beam spots into eight separate plans on the eight phases of 4D-CT, respectively. The doses from different phases were then accumulated onto the planning CT (IAC) through deformable registration using VelocityAI 3.0.1 (Velocity Medical Solutions, Atlanta, GA).

We simulated each dose painting with four different initial phases: EI, EE, MI, and ME. With these four possible initial phases for each painting, there were 10 distinct combinations of initial phases for the two paintings in each fraction, all of which were assessed in this study for all 10 patients.

The entire workflow of the simulation of interplay effect was published in detail [12].

Verification CT and inter-fractional variation

Verification scans reflected the impact of setup, anatomical, and physiological variations on the dose distribution over the course of treatment. We evaluated the interplay effect on the verification scans as described for the initial 4D-CT [12].

Expectation of total dose

The total dose delivered over a number of fractions could be estimated by averaging doses over different initial phases and 4D scans voxel-by-voxel. All dose distributions were mapped onto the same grid through deformable registration before being averaged. For each 4D scan, the doses with different initial phases were given equal weights for averaging purposes [12]. For one fraction, dosimetric values were averaged over four different initial phases for each painting and for different 4D-CT scans. Then for each patient, the averaged doses from different 4D scans were further averaged to estimate the dose delivered over the entire treatment.

Proton pencil beam scanning parameters

Two sets of spot sizes were used based on the hardware available at our institution. Spots with $\sigma \sim 4\text{--}8\text{ mm}$ (in air at the isocenter) were used for all patients. This was the smallest spot size currently used at our facility, which we referred to as small spots. Large spots ($\sigma \sim 6\text{--}16\text{ mm}$) were employed for patients with motion perpendicular to the beam, as the small spots delivery was severely degraded due to interplay.

The simulated energy switching times were: $\tau_{\text{switch}} = 5\text{ s}$, 3 s , 1 s , and 0.5 s . The dosimetric impact of energy switching time on ITV $D_{98\%}$ was assessed via Wilcoxon-signed rank tests.

Results

Figure 1 demonstrated treatment plans across four radiation techniques for a representative patient. PBS provided the

lowest mean dose to heart and lungs, and the lowest maximum dose to the spinal cord for all 10 patients compared to 3D-CRT, IMRT, and DS ($p < 0.05$ for all comparisons), while there was no significant difference in target coverage metrics ($p > 0.05$; Table 1 and Supplementary Table S.II, available online at <http://www.informahealthcare.com>).

Unless otherwise specified, all results were reported for small spots ($\sigma \sim 4\text{--}8\text{ mm}$) and $\tau_{\text{switch}} = 5\text{ s}$, as this would result in the longest treatment and therefore constitutes the worst case scenario for our analysis.

As a representative case, Patient 1 received two verification 4D-CTs (Verification 1 and 2) in addition to the initial scan. In all those scans the breathing amplitudes and periods were consistent (within 5 mm). Coverage on Verification 2 was better than on Verification 1 regardless of initial phase. However, in this 'ideal' patient, coverage was solid regardless of starting phase and between simulated fractions (Table 2). The inadequate coverage in Patients 2 and 5 was discussed below. The corresponding data for the other seven patients were presented in Supplementary Tables S.III–S.IX (available online at <http://www.informahealthcare.com>).

The significant dependence of target coverage (of one fraction) on the initial phase was demonstrated in Table 2 for three patients, and further confirmed by the results from all 32 4D-CT scans of 10 patients. The target coverages with different initial phases were compared via the Wilcoxon-signed rank test. For one painting, the coverages with initial phases of MI or ME were 2% higher than those with initial phases of EI or EE ($p < 0.05$), suggesting the advantage of starting free-breathing treatments at middle phases (e.g. MI and ME) over extreme phases (EI and EE). For two paintings with different initial phases, the relative coverage (percentage of the prescription dose per fraction/painting) is 2% higher than each single painting ($p < 0.05$), confirming the effectiveness of repainting (Supplementary Figure S1, available online at <http://www.informahealthcare.com>).

Out of the 10 patients, eight (80%) showed less than 3% degradation of coverage when averaged over the whole course of treatment, and up to 5% per fraction (Figure 2). The standard deviation of ITV $D_{98\%}$ over the course of treatment was about 0.1% for each of those eight patients. As an outlier, the target of Patient 2 exhibited significant left-right motion (Supplementary Table S.I), which is perpendicular to the anterior radiation field direction. This led to 12% degradation of ITV $D_{98\%}$ per fraction and 9% over the course of treatment (Table 2; Figure 2). This dose degradation was effectively mitigated to $\sim 1\%$ for the whole treatment course and $\sim 3\%$ per fraction by applying large spots (Figure 2). Another outlier was Patient 5. This patient, who was being treated for refractory primary mediastinal large B-cell lymphoma that had progressed after second line chemotherapy, developed a pericardial effusion during the course of treatment from progressive disease, which resulted in large ($\sim 2\text{ cm}$) inter-fractional target motion. Specifically, the relative $D_{98\%}$ of ITV calculated on one of the verification CTs (Verification 1) was below 20%, regardless of starting phase (Table 2).

The 4D-evaluated results of mean dose to lung, maximum dose to heart, mean dose to heart, and maximum dose to spinal cord were within 10% of the prescribed dose for all

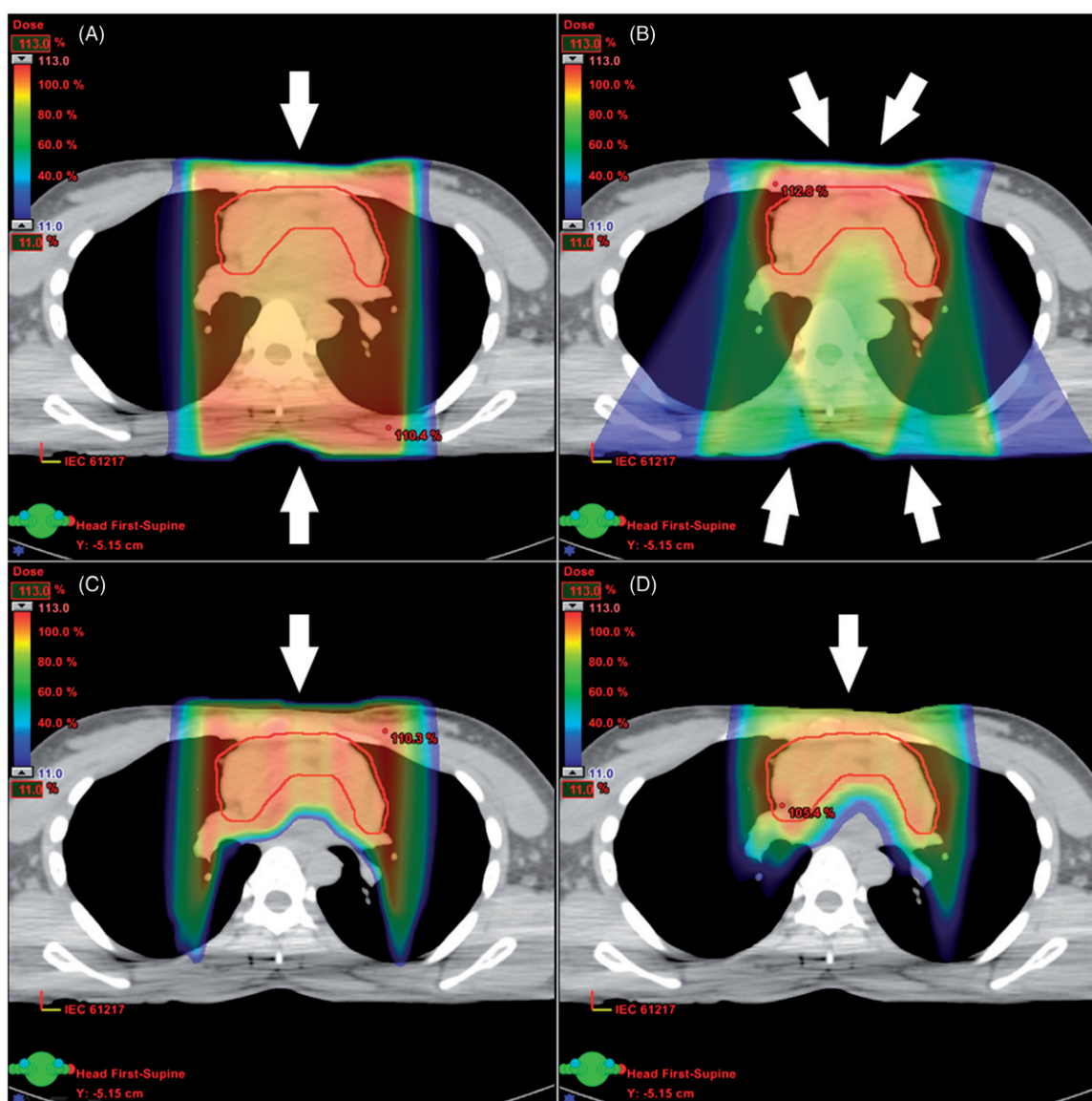


Figure 1. Three-dimensional conformal radiotherapy (A), intensity-modulated radiotherapy (B), proton double scattering (C), and pencil beam scanning (D) treatment plans for a patient. The contour shown is the internal target volume.

patients except Patients 2 and 5 (Figure 3). The maximum doses to spinal cord for Patients 2 and 5 were significantly larger than in the nominal plan: increases of 8.9 Gy (RBE) for Patient 2 (with small spots) and 4.7 Gy (RBE) for Patient 5. That was attributable to the left-right motion of the trachea, which led to significant overshooting of the proton beam onto the spinal cord, an issue that was also observed with DS proton therapy.

For target coverage robustness ($D_{98\%}$), no statistically significant difference was observed for the four different energy switching times evaluated via two-sided Wilcoxon-signed rank tests ($p > 0.05$), with the maximum difference $< 1.5\%$. The values of average difference in coverage between any two switching times were also small ($< 0.5\%$).

Discussion

We have demonstrated how to clinically implement PBS for MLs, which we show is dosimetrically superior to photon and

DS proton therapy. Free-breathing PBS treatment of ML is feasible using a small spot size when the motion is limited to the direction along the beam and it requires a larger spot size when the motion is present in the direction perpendicular to the beam direction. For our facility, we apply small spots for motion < 5 mm.

Motion values reported in Table 1 are the maximum displacements. For ML, the target may extend inferiorly to the level of heart. Usually the tip of target that extends inferiorly has the largest motion magnitude along superior-inferior (SI) direction. However, the volume of target at the tip level relative to the whole target volume is very limited, as most of the target is superior to the heart. Moreover, inferior to the target is heart, not lung; therefore no large heterogeneities are involved. The proton stopping power for heart is much closer to the target than lung. As a result, SI motion of the inferior tip of target does not lead to significant undershoot or overshoot of the proton beam.

Table 1. Dosimetric endpoints for target and organs at risk.

	Median (95% confidence interval)			
	PBS	DS	IMRT	3D-CRT
ITV				
$D_{98\%}$	97.0 (97.0–98.6)%	97.0 (97.0–97.0)%	97.0 (97.0–97.0)%	97.0 (97.0–97.0)%
$D_{95\%}$	97.8 (97.6–99.2)%	98.0 (98.0–99.0)%	97.8 (97.4–98.2)%	98.0 (97.5–98.5)%
$V_{95\%}$	99.9 (99.5–100.0)%	99.8 (99.0–100.0)%	100.0 (99.4–100.0)%	99.9 (99.6–100.0)%
Lungs				
$D_{\text{mean}}/\text{Gy(RBE)}$	5 (2–9)	6 (3–11)*	9 (4–12)*	11 (6–18)*
$V_{30\text{Gy(RBE)}}$	2 (1–7)%	7 (2–15)%*	1 (0–3)%*	10 (0–40)%*
$V_{20\text{Gy(RBE)}}$	11 (5–23)%	18 (7–31)%*	19 (6–25)%*	29 (14–47)%*
$V_{10\text{Gy(RBE)}}$	20 (10–30)%	25 (10–40)%*	35 (13–49)%*	37 (17–58)%*
$V_{5\text{Gy(RBE)}}$	23 (11–43)%	30 (13–51)%*	56 (25–73)%*	44 (21–68)%*
Heart				
$D_{\text{mean}}/\text{Gy(RBE)}$	5.8 (0.4–15.9)	7.4 (0.7–16.3)*	10.4 (0.9–17.5)*	12.7 (1.9–25.8)*
$D_{\text{max}}/\text{Gy(RBE)}$	32 (31–35)	34 (31–37)*	34 (30–36)*	33 (31–34)*
$V_{30\text{Gy(RBE)}}$	7 (0–30)%	15 (0–43)%*	6 (0–26)%	16 (1–35)%*
$V_{20\text{Gy(RBE)}}$	15 (0–49)%	22 (2–50)%*	29 (0–46)%*	38 (3–83)%*
$V_{10\text{Gy(RBE)}}$	21 (1–56)%	25 (3–54)%*	36 (1–73)%*	42 (5–90)%*
$V_{5\text{Gy(RBE)}}$	25 (2–60)%	28 (4–57)%	46 (3–91)%*	45 (6–93)%*
Spinal cord				
$D_{\text{max}}/\text{Gy(RBE)}$	14 (1–23)	26 (10–33)*	27 (24–28)*	32 (30–34)*
Breasts				
$D_{\text{mean}}/\text{Gy(RBE)}$	0.5 (0.5–3.1)	0.6 (0.6–3.2)	1.0 (0.8–2.7)*	1.0 (1.0–3.7)
$D_{\text{max}}/\text{Gy(RBE)}$	28.0 (27.8–28.0)	33 (31–34)*	33 (31–35)*	33.7 (33.5–33.8)*

IMRT: intensity-modulated radiotherapy; ITV: internal target volume; DS: double scattering; PBS: pencil beam scanning; 3D-CRT: three-dimensional conformal radiotherapy.

*Statistically significantly higher than PBS ($p < 0.05$; Wilcoxon-signed rank test).

Table 2. Internal target volume coverage (relative $D_{98\%}$) of three selected cases obtained on different 4D-CT scans (Initial, Verification 1, and Verification 2). We simulate each dose painting with four different initial phases: EI, EE, MI and ME. With these four possible initial phases for each painting, there are 10 distinct combinations of initial phases for the two paintings in each fraction.

Initial phases	Patient 1			Patient 2			Patient 5		
	Initial	Verification 1	Verification 2	Initial	Verification 1	Verification 2	Initial	Verification 1	Verification 2
EE + EE	95.5%	90.5%	94.7%	83.0%	76.6%	79.9%	93.9%	19.6%	85.0%
EE + EI	96.2%	92.9%	94.9%	95.1%	82.0%	84.9%	95.3%	19.6%	87.2%
EI + EI	95.6%	91.2%	94.0%	91.0%	82.2%	82.4%	93.1%	19.3%	87.3%
EE + ME	96.8%	93.1%	96.0%	89.5%	80.5%	84.7%	95.3%	18.7%	85.7%
EI + ME	96.9%	94.3%	95.4%	97.4%	81.9%	84.5%	95.3%	18.5%	86.4%
ME + ME	96.2%	93.5%	95.2%	95.0%	80.6%	85.1%	93.8%	17.7%	84.2%
EE + MI	96.6%	94.1%	95.2%	91.7%	81.3%	84.4%	95.3%	19.1%	86.0%
EI + MI	96.3%	94.3%	95.1%	94.7%	82.0%	83.4%	95.1%	19.0%	86.8%
ME + MI	97.0%	95.4%	96.0%	97.4%	81.3%	85.1%	95.2%	18.1%	85.1%
MI + MI	95.8%	94.1%	95.0%	96.3%	81.4%	83.9%	94.7%	18.6%	85.4%

EE: end of exhalation; EI: end of inhalation; ME: middle of exhalation; MI: middle of inhalation.

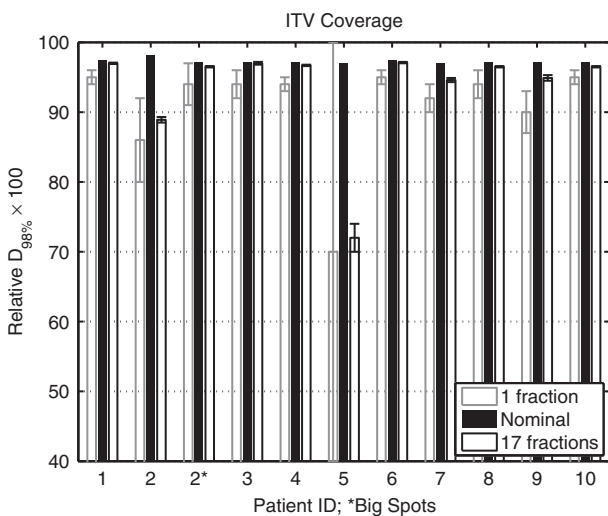


Figure 2. ITV coverage for 10 patients. The nominal values are those from the original plans on initial average CT. Each error bar is one standard deviation above and below the mean. *Large spots (~6–16 mm σ) were applied to Patient 2, who exhibited target motion perpendicular to the proton beam (>5 mm). ITV: internal target volume.

In this study, for all patients, the median reduction in mean heart dose (MHD) with PBS compared with any other modality ranged from 1 to 7 Gy. In breast cancer survivors, Darby et al. [18] demonstrated an increased relative risk of major coronary events with mean doses to the heart by 7.4% per Gy with no threshold. Similar results were noted in Hodgkin lymphoma survivors, with an excess relative risk of 7.4% per Gy, which would translate to a risk reduction that ranges from 7% to 65% using PBS compared to other modalities [19]. The dose limit for specific cardiac structures like coronary arteries or valves has not been well characterized, but the superior conformality of PBS compared to DS proton therapy could potentially be used to avoid specific cardiac substructures, depending on individual anatomy.

For lung doses, there are two important toxicities to consider: radiation pneumonitis and lung cancer risk. Mean lung doses (MLD) below 13.5 Gy and $V_{5\text{Gy}}$ below 55% are associated with a low incidence of clinically significant pneumonitis; however, the risk is higher in patients with relapsed/refractory disease [20]. The incrementally decreased lung dose with PBS

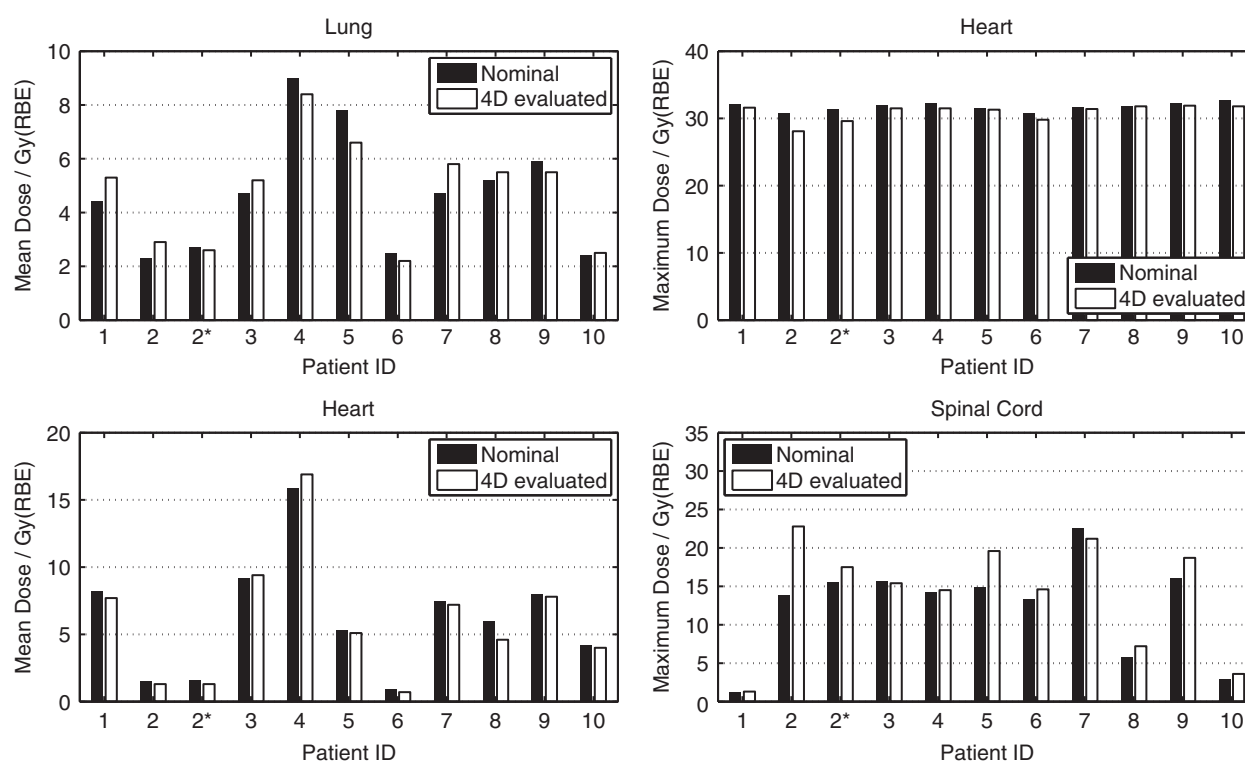


Figure 3. Comparison of 4D-evaluated dosimetric endpoints for lung, heart and spinal cord. *Large spots ($\sim 6\text{--}16\text{ mm } \sigma$) were applied to Patient 2, who exhibited target motion perpendicular to the proton beam ($>5\text{ mm}$).

may not be clinically significant with respect to pneumonitis in the majority of cases that use involved-site RT volumes. However, the risk of lung cancer is an important variable to consider for long-term mortality. Decreasing lung dose by 15–50% using PBS compared to other modalities may help decrease the risk of lung cancer, an effect that is multiplied in smokers [21].

Although the spinal cord doses are generally low with lymphoma treatment, there is a possibility that these patients will receive another course of radiation treatment in the future in the relapsed setting. Therefore we report the cord dose to illustrate that when proton beams are employed, cord dose limitations are removed for patient reirradiation purposes.

Our PBS plan employed a single anterior field for each patient, while anterior-posterior opposed PBS fields were used in other studies [4,17]. As ML targets usually are anterior and tend to be shallow, posterior PBS fields may unnecessarily increase heart dose. In some instances, the use of posterior beams to treat posterior mediastinal disease can spare breast tissue and anterior cardiac structures.

While changes in the energy switching time (0.5 s, 1 s, 3 s, and 5 s) do not affect the target coverage in general, there is a possibility that the beam scanning is synchronized with the breathing cycles, leading to undesired interplay. This ‘synchronization’ of beam scanning and breathing cycles was observed in one of the 4D scans for Patient 2 [12]. In this scenario, the dose may be delivered only during some particular phases, with other phases ‘missed’ during a painting.

However, the actual time spent within each iso-energy layer varies from layer to layer; and a patient’s breathing period is not exactly the same from one cycle to another,

which is uncorrelated to the beam scanning. With more than 10 iso-energy layers for a typical field, it is very likely that every breathing phase will receive some dose from at least one layer. Thus the undesired synchronization (between beam scanning and breathing cycles) should be very unlikely. (According to all the scenarios simulated in this study, during one dose painting, the probability of synchronization is 0.04 ± 0.01 .) Furthermore, as a patient’s respiratory trace slightly varies from day to day, any missed volume from a single phase is unlikely to persist throughout the treatment.

For energy switching time of 1 s or less, the time interval between the beginnings of consecutive layers will almost always be less than the breathing period, so synchronization would be avoided. That is to say, consecutive layers will never start at the same breathing phase. Therefore, switching times of $<1\text{ s}$ are potentially advantageous in avoiding synchronization as well as increasing patient throughput.

For free-breathing treatments, different dose paintings will generally start at different breathing phases. Even in the presence of synchronization of beam scanning and breathing cycles, the phase that was totally missed during one painting may be covered in the next painting. Eventually, the synchronization effect, which happens only with a very small probability, would be washed out throughout the course of treatment. However, the impact of the magnitude of τ_{switch} could be more significant for hypofractionated radiation treatments.

Case 5, a patient with refractory lymphoma, exhibited significant inter-fractional anatomical changes due to development of pericardial effusion. This patient had primary mediastinal large B-cell lymphoma that was refractory to initial chemotherapy and then progressed after second line

chemotherapy at the start of radiation. Hence, he was at high risk of progressing while on radiation. Adaptive replanning would be required for this patient due to the unexpected anatomical variation captured by verification CT scan, which had the largest impact on the delivered dose distribution. It underlines the importance of volumetric imaging evaluation in patients with active disease, such as verification CT or cone-beam CT, throughout the course of treatment.

We have used deformable registration in VelocityAI to facilitate dose accumulation. The registration accuracy has been validated by a number of recent studies (e.g. [22]), however, there is a lack of direct validation of dose accumulation. While deformable physical phantom can provide the ground truth for validation of deformable registration, deformable phantom with an array of detectors would be needed in order to directly validate the accumulation of dose distribution. One recent attempt is from Graves et al. [23], who proposed a deformable phantom in which diodes can be placed. This type of research is warranted in order to support the widely used 4D dose calculation schemes across photon and proton radiation therapy [24,25].

To conclude, this study demonstrates that PBS plans significantly spare the OARs relative to 3D-CRT, IMRT, and DS plans, and identifies requirements for robust free-breathing ML PBS treatments, such as the use of repainting and/or beam spots with σ larger than motion magnitude perpendicular to the beam.

Acknowledgments

This work was supported by Ion Beam Applications S.A., Louvain-la-Neuve, Walloon Brabant, Belgium (IBA). The authors would like to thank Olivier De Wilde and Guillaume Janssens from IBA for their contribution.

Disclosure statement

Dr. Both received a grant from IBA for the project. Drs. Zeng, Plastaras, Tochner, Hill-Kayser, and Hahn and Mr. James have no conflicts.

References

- Li J, Dabaja B, Reed V, Allen PK, Cai H, Amin MV, et al. Rationale for and preliminary results of proton beam therapy for mediastinal lymphoma. *Int J Radiat Oncol Biol Phys* 2011;81:167–74.
- Hoppe BS, Flampouri S, Su Z, Latif N, Dang NH, Lynch J, et al. Effective dose reduction to cardiac structures using protons compared with 3DCRT and IMRT in mediastinal Hodgkin lymphoma. *Int J Radiat Oncol Biol Phys* 2012;84:449–55.
- Knausl B, Lutgendorf-Caucig C, Hopfgartner J, Dieckmann K, Kurch L, Pelz T, et al. Can treatment of pediatric Hodgkin's lymphoma be improved by PET imaging and proton therapy? *Strahlenther Onkol* 2013;189:54–61.
- Maraldo MV, Brodin NP, Aznar MC, Vogelius IR, Munck af Rosenschöld P, et al. Estimated risk of cardiovascular disease and secondary cancers with modern highly conformal radiotherapy for early-stage mediastinal Hodgkin lymphoma. *Ann Oncol* 2013;24:2113–18.
- Dowdell S, Grassberger C, Sharp GC, Paganetti H. Interplay effects in proton scanning for lung: a 4D Monte Carlo study assessing the impact of tumor and beam delivery parameters. *Phys Med Biol* 2013;58:4137–56.
- ICRU. CRU Report 78: Prescribing, recording, and reporting proton-beam therapy. *J ICRU* 2007;7:1–210.
- Bortfeld T, Jokivarsi K, Goitein M, Kung J, Jiang SB. Effects of intra-fraction motion on IMRT dose delivery: statistical analysis and simulation. *Phys Med Biol* 2002;47:2203–20.
- Phillips MH, Pedroni E, Blattmann H, Boehringer T, Coray A, Scheib S. Effects of respiratory motion on dose uniformity with a charged particle scanning method. *Phys Med Biol* 1992;37:223–34.
- Seco J, Robertson D, Trofimov A, Paganetti H. Breathing interplay effects during proton beam scanning: simulation and statistical analysis. *Phys Med Biol* 2009;54:N283–94.
- Zenkhusen SM, Pedroni E, Meer D. A study on repainting strategies for treating moderately moving targets with proton pencil beam scanning at the new Gantry 2 at PSI. *Phys Med Biol* 2010;55:5103–21.
- Bassler N, Jakel O, Sondergaard CS, Petersen JB. Dose- and LET-painting with particle therapy. *Acta Oncol* 2010;49:1170–6.
- Zeng C, Plastaras JP, Tochner ZA, White BM, Hill-Kayser CE, Hahn SM, et al. Proton pencil beam scanning for mediastinal lymphoma: the impact of interplay between target motion and beam scanning. *Phys Med Biol* 2015;60:3013–29.
- Illidge T, Specht L, Yahalom J, Aleman B, Berthelsen AK, Constine L, et al. Modern radiation therapy for nodal non-Hodgkin lymphoma-target definition and dose guidelines from the International Lymphoma Radiation Oncology Group. *Int J Radiat Oncol Biol Phys* 2014;89:49–58.
- Specht L, Yahalom J, Illidge T, Berthelsen AK, Constine LS, Eich HT, et al. Modern radiation therapy for Hodgkin lymphoma: field and dose guidelines from the International Lymphoma Radiation Oncology Group (ILROG). *Int J Radiation Oncology Biol Phys* 2014;89:854–62.
- Paganetti H, editor. *Proton Therapy Physics*. Boca Raton: CRC Press; 2011.
- Goitein M. Calculation of the uncertainty in the dose delivered during radiation therapy. *Med Phys* 1985;12:608–12.
- Maraldo MV, Brodin NP, Aznar MC, Vogelius IR, Munck af Rosenschöld P, Petersen PM, et al. Doses to head and neck normal tissues for early stage Hodgkin lymphoma after involved node radiotherapy. *Radiother Oncol* 2014;110:441–7.
- Darby SC, Ewertz M, McGale P, Bennet AM, Blom-Goldman U, Bronnum D, et al. Risk of ischemic heart disease in women after radiotherapy for breast cancer. *N Engl J Med* 2013;368:987–98.
- van Nimwegen FA, Schaapveld M, Cutter DJ, Janus CPM, Kroel ADG, Hauptmann M, et al. Radiation dose-response relationship for risk of coronary heart disease in survivors of Hodgkin lymphoma. *J Clin Oncol* 2015;34:235–43.
- Pinnix C, Smith GL, Milgrom S, Osborne EM, Reddy RP, Akhtari M, et al. Predictors of radiation pneumonitis in patients receiving intensity modulated radiation therapy for Hodgkin and non-Hodgkin lymphoma. *Int J Radiat Oncol Biol Phys* 2015;92:175–82.
- Travis LB, Gospodarowicz M, Curtis RE, Clarke EA, Andersson M, Glimelius B, et al. Lung cancer following chemotherapy and radiotherapy for Hodgkin's disease. *J Natl Cancer Inst* 2002;94:182–92.
- Nie K, Chuang C, Kirby N, Braunstein S, Pouliot J. Site-specific deformable imaging registration algorithm selection using patient-based simulated deformations. *Med Phys* 2013;40:041911.
- Graves YJ, Smith AA, McIlvina D, Manilay Z, Lai YK, Rice R, et al. A deformable head and neck phantom with in-vivo dosimetry for adaptive radiotherapy quality assurance. *Med Phys* 2015;42:1490–7.
- Kuo HC, Mah D, Chuang KS, Wu A, Hong L, Yaparpalvi R, et al. A method incorporating 4DCT data for evaluating the dosimetric effects of respiratory motion in single-arc IMAT. *Phys Med Biol* 2010;55:3479–97.
- Grassberger C, Dowdell S, Lomax A, Sharp G, Shackelford J, Choi N, et al. Motion interplay as a function of patient parameters and spot size in spot scanning proton therapy for lung cancer. *Int J Radiat Oncol Biol Phys* 2013;86:380–6.